

Full Length Article

Effects of natural micro-fracture morphology, temperature and pressure on fluid flow in coals through fractal theory combined with lattice Boltzmann method

Qian Li^{a,b}, Dameng Liu^{a,b}, Yidong Cai^{a,b,*}, Bo Zhao^c, Yuejian Lu^{a,b}, Yingfang Zhou^d

^a School of Energy Resources, China University of Geosciences, Beijing 100083, China

^b Coal Reservoir Laboratory of National Engineering Research Center of CBM Development & Utilization, China University of Geosciences, Beijing 100083, China

^c School of Water Resources and Environment, China University of Geosciences, Beijing 100083, China

^d School of Engineering, Fraser Noble Building, King's College, University of Aberdeen, AB24 3UE Aberdeen, UK



ARTICLE INFO

Keywords:

Coal
Micro-fractures morphology
Permeability
Fractal theory
Lattice Boltzmann method

ABSTRACT

The fluid flow behaviors during the production of coalbed methane (CBM) are generally restricted by the pre-existing natural fractures in coal seams. To better understand the effect of natural micro-fracture morphology on the flow capability, nine coals collected from Ordos Basin were subjected to optical microscope observations to obtain micro-fractures morphology. And then, the box-counting method (BCM) was used to quantify the complexity of the micro-fracture network planar distribution. Besides, the lattice Boltzmann method (LBM) was adopted to simulate the flow in the complex micro-fracture network under different pressures and temperatures. Finally, factors affecting the flow capability in micro-fracture were elaborated. The results show that the micro-fractures generally present dendritic, reticular, filamentous and orthogonal structures. The natural micro-fracture morphology has a remarkable impact on flow behavior, in which the presence of dominant channels with a length of $\sim 498.26 \mu\text{m}$ and a width of $\sim 10.96 \mu\text{m}$ has a significant contribution to permeability, while the orthogonal micro-fracture network normally is not conducive to fluid flow. The fractal dimension extracted from the nine coals varies from 1.321 to 1.584, and the permeability calculated from LBM method varies from 0.147 to 0.345 D; in contrast to other studies, a non-monotonic change, an inverted U-shaped, of permeability on fractal dimension was observed. Moreover, permeability decreases as pressure increases and increases with increasing temperature due to the physical properties of methane and coal matrix. Therefore, this work may contribute to understanding the process of hydrofracturing and hydrothermal methods for improving CBM reservoirs during enhancing CBM recovery.

1. Introduction

Coalbed methane (CBM) is an essential component of the unconventional energy system due to its huge reserves, the reservoir of which is deemed as a dual-porous medium with pores in matrix and fractures/cleats [1–3]. Pores are generally associated with the processes of gas storage, desorption and diffusion [4]. For fractures, composed by micro-fractures and macro-fractures, they are the most important physical attribute governing gas flow in a CBM reservoir [5,6]. Generally speaking, natural fractures primarily contributed to the permeability of coal, while the pores in coal matrix have very limited influence [7]. Extensive works including experiments and numerical simulations have been conducted to understand the performance of micro-fracture with

the width at micron scale due to its importance on CBM production [8–24]. Multiple experimental methods can be used to characterize micro-fractures properties, including low-field nuclear magnetic resonance (NMR) [8,9], X-ray computed micro-tomography (X-ray μCT) [10–12] and the classic optical microscopy [13]. NMR is a non-destructive measurement and has been adopted successfully to detect and quantify the pore-fracture structure of coals [8], where the T_2 spectrum larger than 100 ms represents micro-fracture [9]. However, the detailed morphological features of micro-fracture are not accessible through NMR. X-ray μCT can provide realistic three-dimensional digital images and different components reconstruction [10–12]. Jenkins et al. [12] utilized X-ray μCT to dynamically measure the deformation behavior of tested rock under various loading conditions. However, X-ray μCT is expensive and time-consuming. Compared with the above

* Corresponding author at: School of Energy Resources, China University of Geosciences, Beijing 100083, China.

E-mail address: yidong.cai@cugb.edu.cn (Y. Cai).

Nomenclatures			
R	length of boxes	ρ	density
D	fractal dimension	\mathbf{u}	fluid velocity
$N(r)$	the number of boxes required to completely cover the image	ν	kinematic viscosity
FP	fracture porosity	n	spatial dimension
f	distribution function	b	number of discrete velocity vectors
x	position of the particles	c_s	sound speed
t	time	c	lattice velocity
δ_x	lattice size	R	gas constant
δ_t	time step	T	temperature
τ	relaxation time	ω_i	weight coefficient
e_i	the discrete propagation velocity vector in i direction	K	intrinsic permeability with physical unit
$f_i^{(eq)}$	the equilibrium distribution function	K_{LBM}	permeability simulated by LBM
		L	the real scale of coal sample
		L_{LBM}	the scale of LBM
		U	normalized streamwise velocity

techniques, the micro-fracture morphology observation by optical microscopy is not only economically suitable but also easy to obtain clear morphologies [13]. Besides, the fractal dimension can extend the qualitative description of the micro-fracture network to a quantitative description, which quantifies its complexity of distribution [14,15]. The box-counting method (BCM) is one of the most popular algorithms [16,17] to acquire the complexity, namely fractal dimension, through the images of pore-fracture structure. Herein, the BCM will be utilized to quantify the complexity of micro-fractures. On the other hand, direct numerical methods including finite difference method (FDM) [18], finite element method (FEM) [19] and finite volume method (FVM) [20] can be effectively adopted to simulate the flow behavior in micro-fracture networks. But these traditional simulation methods on the basis of Navier-Stokes equations require complicated meshing process to define the simulation domain and are challenging to solve complex geometric boundaries and have low parallel efficiency [18–20]. The lattice Boltzmann method (LBM), as a typical mesoscopic method, has a strong advantage in simulating the flow behavior of porous media with irregular boundaries [21,22]. For example, Wang et al. [23] decomposed the three-dimensional fracture geometry into primary and secondary roughness through wavelet analysis, and investigated the role of the latter in the flow of rock fractures using LBM. And Zhao et al. [24] adopted LBM to discuss the effect of structure, surface roughness and aperture on flow in constructed fracture networks with rough surfaces.

The previous works on coal fractures/cleats can be classified into two parts: characterization of micro-fracture networks [8–13] and the exploration of gas flow behavior in the micro-fracture networks [18–24]. It is significant for understanding the effect of natural fracture network on permeability through investigating the characteristics and distribution of natural fractures in coal. Besides, owing to the complexity of the natural fracture network in coal, much related work has performed flow simulation in the fracture network constructed by algorithms such as Voronoi tessellations method [24,25] and Fracture

Pipe Network Model (FPNM) [26], whereas rare researches have been conducted on the real complex natural fracture networks with specific morphologies. Many studies adopted an idealistic tube model with a circular cross-section to simplify the flow simulation [27,28]. However, in most cases, the shape of micro-fractures is non-circular and irregular in coal, which is much complicated. Therefore, Yuan et al. [29] compared the realistic shape with the permeability characteristics of circle, square and equilateral triangular cross-sections, which found that the permeability of the network with circle cross-section is the highest, followed by the realistic shape, and the final are square and equilateral triangular. This finding corroborates the importance of accurately acquiring morphological features in micro-fracture networks.

In this study, we aim to investigate the flow behavior in natural micro-fractures with various morphologies under different pressures and temperatures. To detailed address the flow behavior in micro-fractures, the specific morphologies of natural micro-fractures were firstly obtained by optical microscopy. And then, the BCM was used to quantify the complexity of the natural micro-fracture network. After that, the LBM was applied to simulate the flow behavior in the natural micro-fracture network with specific morphologies in coals, and the controlling factors were revealed. This study may provide insights into the flow mechanisms of natural micro-fracture networks with complex morphologies in unconventional reservoirs.

2. Methodology and validation

2.1. Coal sampling and basic analysis

Nine coal blocks ($30 \times 30 \times 30 \text{ cm}^3$) with different coal ranks were selected from the eastern Ordos Basin, north China. The maximum vitrinite reflectance ($R_{o, \max}$) and maceral composition were carried out with a Leitz MPV-III microscope photometer following the Chinese National Standard of GB/T 6948–1998. The $R_{o, \max}$ varies from 0.62% to

Table 1
Sample information and basic parameters of the selected coals.

Sample no.	Basin	$R_{o, \max}$ (%)	Maceral and mineral (%)				Fracture porosity (%)
			Vitrinite	Inertinite	Exinite	Mineral	
F1	Ordos	0.62	65.4	21	5.3	8.3	4.53
F2		0.65	66.2	24.9	1.4	7.5	5.35
F3		0.68	90.1	4.5	4.4	1	3.54
F4		0.89	66.9	25.6	5.9	1.6	2.45
F5		1.27	90.2	8.3	0	1.5	9.05
F6		1.27	82.3	14.7	0	3	7.50
F7		1.36	82.2	15.2	2.4	0.2	9.11
F8		1.58	84.0	11.6	0.6	3.8	4.64
F9		1.78	84.4	7.9	3.1	4.6	2.41

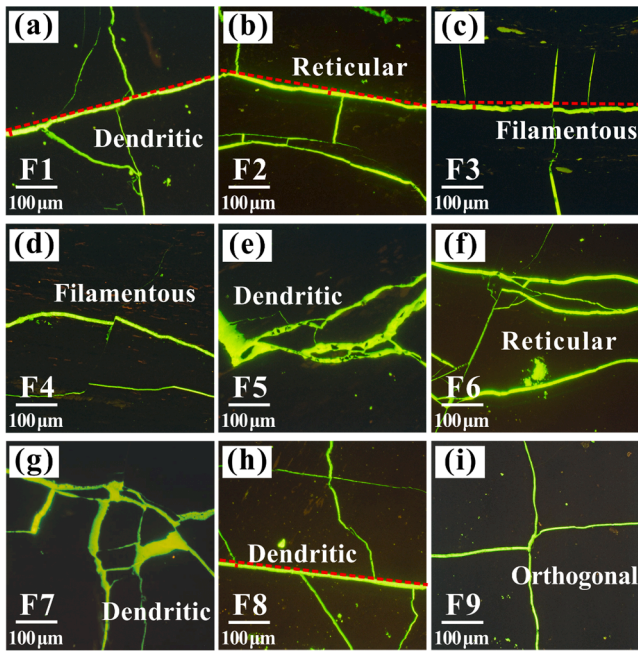


Fig. 1. Different micro-fracture morphologies of selected samples obtained by optical microscope, which varied involving dendritic, reticular, filamentous and orthogonal etc. The red dotted lines are the dominant channels mentioned in section 4.1. (For interpretation of the references to colour in this figure legend, the reader is referred to the web version of this article.)

1.78% as shown in Table 1, which may indicate the variable inner micro-fractures existed [30]. Coal macerals were tested by the point counting technique according to the scheme of the International Committee for Coal and Organic Petrology [31]. The coal composition differs, with vitrinite of 65.4–90.2%, inertinite of 4.5–25.6%, exinite of 0–5.9% and mineral being 0.2–8.3%. Natural micro-fractures of coals selectively develop in macerals/submacerals, for example, micro-fractures develop well in the telocollinites while others including the desmocollinite, vitrodetrinite, inertodetrinite and semifusinite are not conducive to micro-fractures development [30].

2.2. Micro-fractures characterization by optical microscopy

The morphological characteristics of the natural micro-fractures can be clearly observed by optical microscopy. The specific preparation process of used coals is as follows: first a certain proportion of resin and paraffin was melted, and then was poured into the micro-fractures of coal. After that, the coals were cut and polished into the blocks with the area of $\sim 3 \times 3 \text{ cm}^2$. To the end, LABORLUX 12 POL optical microscopy (Leitz Company of Germany) was utilized to observe the natural micro-fractures performance including the morphological characteristics. Natural micro-fractures morphologies with the image resolution of $0.4937 \mu\text{m}$ were achieved, which contain various shapes involving dendritic, reticular, filamentous and orthogonal structure as shown in Fig. 1. The natural dendritic micro-fracture network is mostly composed of a backbone and several branches extending out (see Fig. 1a, e, g and h). The natural reticular micro-fracture network can be divided into regular type (Fig. 1b) and disorganized type (Fig. 1f), which have the common feature of more than two main channels and the part of branches connecting the main channels, and their difference is whether the channel is curved and disorganized. The natural filamentous micro-fracture network primarily has a channel similar to a ribbon with weak connectivity. Comparatively, the orthogonal micro-fracture network is easy to distinguish, which has a pair of orthogonal channels.

After collecting the images, these images need to be preprocessed including noise reduction and image segmentation. First to reduce noise,

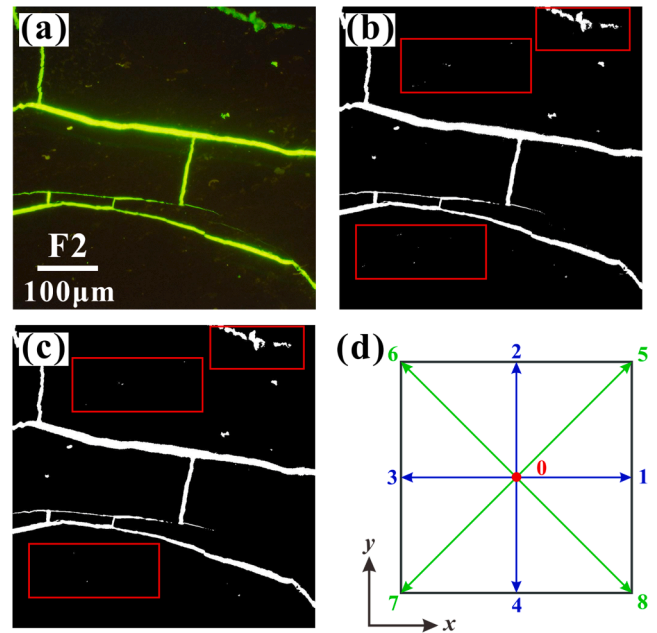


Fig. 2. The results after threshold segmentation and the discrete velocity of D2Q9 model. (a) is the initial image; (b) and (c) are images before and after noise reduction, respectively. Careful observation shows that the noise in the red rectangular frame of (c) is significantly less than that in (b), and the edge of the micro-fracture in (c) is smoother after noise reduction. (d) is the discrete velocity of D2Q9 model. (For interpretation of the references to colour in this figure legend, the reader is referred to the web version of this article.)

which normally due to the limitations of the experimental equipment, herein the median filter is chosen to reduce the noise for studied images (Fig. 2). And then the images need to be segmented by Otsu algorithm, which has been proved to be an effective and conciseness threshold segmentation method [16,32]. After thresholding, the micro-fractures were distinguished from the background in the selected coals. As shown in Fig. 2c, black is the micro-fracture and white is the coal matrix in the binary images. Detailed observation shows that the noise in the red rectangular frame of Fig. 2c is significantly less than that in Fig. 2b; what's more the edge of the micro-fracture in Fig. 2c is smoother after noise reduction.

2.3. Fractal theory applied for micro-fractures network

The fractal theory proposed by Mandelbrot [33] can be used to evaluate the natural porous properties such as coals and shales. The fractal dimension, the characteristic parameter of fractal theory, can effectively quantify the complexity of pore-fracture structure. For a two-dimensional (2D) system, the fractal dimension changes from 1 to 2; a larger the fractal dimension represents a more complicated fracture system. Previous research has been demonstrated that fractal dimensions of pore-fracture structure can be acquired from images by the BCM [16,17,34,35]. In this study, the fractal dimensions of obtained 2D micro-fracture images were determined by the BCM to quantify the complexity of the micro-fracture distribution. The details of BCM have been listed in our latest work [35], and the following is a brief description:

By covering a binary image with boxes of length r , the fractal dimension D can be estimated as:

$$D = -\lim_{r \rightarrow 0} \frac{\log(N(r))}{\log(r)} \quad (1)$$

where $N(r)$ is the number of boxes required to cover the complete image. The side length r of the box needs to be assigned a series of values, and

the number of boxes $N(r)$ required to cover the image is counted. Then a set of $[\log(r), \log(N(r))]$ values of each sample are plotted in the coordinate system with the abscissa of $\log(r)$ and the ordinate of $\log(N(r))$. The slope is determined by the least square fitting method, which is the fractal dimension D .

Within the calculation process, we adopted the method proposed by Wu et al. [36] to avoid boundary effects, using the common divisors of the length and width of the image as a series of box sizes.

In addition, the fracture porosity (FP) of each sample was calculated following Eq. (2), as listed in Table 1.

$$FP = \frac{\text{fracture pixel}}{\text{total pixel}} \times 100\% \quad (2)$$

2.4. Flow simulation using lattice Boltzmann method

The flow simulation was carried out based on the Bhatnagar Gross Krook (BGK) model [37], which is the most widely used model. The distribution functions f_i can be expressed as:

$$f_i(x + e_i \delta_t, t + \delta_t) - f_i(x, t) = -\frac{1}{\tau} [f_i(x, t) - f_i^{(eq)}(x, t)] \quad (3)$$

where x is the position of the particles; t is time; δ_t is the time step; τ is the relaxation time; e_i is the discrete propagation velocity vector in i direction, $f_i^{(eq)}$ is the equilibrium distribution function of e_i for density ρ and fluid velocity u .

The relaxation time τ is adopted:

$$\tau = \frac{\nu}{c_s^2 \delta_t} + \frac{1}{2} \quad (4)$$

where ν is the kinematic viscosity; $c_s = \sqrt{RT} = c/\sqrt{3}$ is the sound speed, in which R is the gas constant and T is the temperature.

The DnQb model (n is the spatial dimension and b is the number of discrete velocity vectors) proposed by Qian et al. [38] is the most representative. We utilize the D2Q9 model (see Fig. 2d), and its equilibrium distribution function $f_i^{(eq)}$ can be expressed as:

$$f_i^{(eq)} = \omega_i \rho \left[1 + \frac{e_i \cdot u}{c_s^2} + \frac{(e_i \cdot u)^2}{2c_s^4} - \frac{u \cdot u}{2c_s^2} \right] \quad (5)$$

where $c = \delta_x / \delta_t$ is the lattice velocity, and both the lattice size δ_x and time step δ_t are set to 1. The e_i and weight coefficient ω_i are defined as:

$$e_i = c \begin{bmatrix} 0 & 1 & 0 & -1 & 0 & 1 & -1 & -1 & 1 \\ 0 & 0 & 1 & 0 & -1 & 1 & 1 & -1 & -1 \end{bmatrix} \quad (6)$$

$i = 0, 1, \dots, 8$

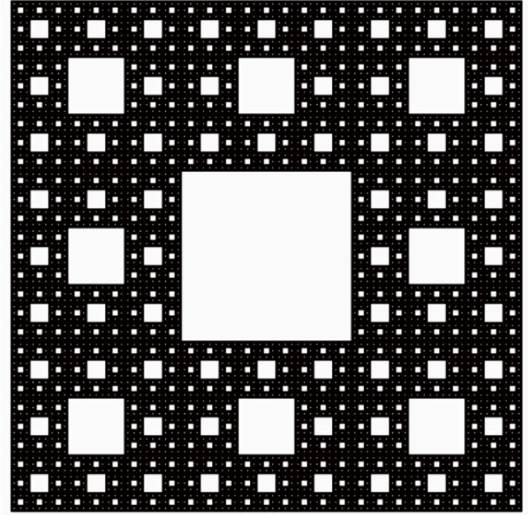
$$\omega_i = \begin{cases} 4/9 & i = 0 \\ 1/9 & i = 1 - 4 \\ 1/36 & i = 5 - 8 \end{cases}$$

For isothermal gas flow, the macroscopic parameters, such as density and momentum, can be determined as:

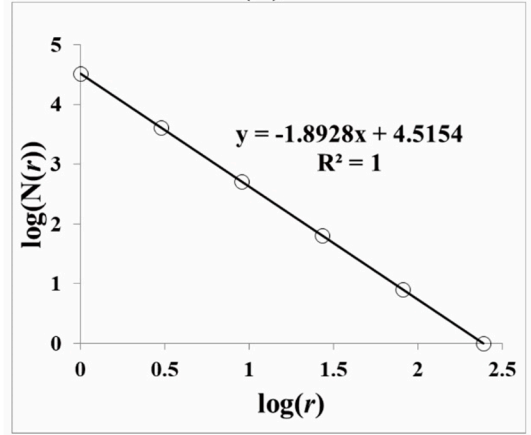
$$\rho = \sum_i f_i \rho u = \sum_i e_i f_i \quad (7)$$

The pressure boundary conditions are applied to the inlet and outlet. The stationary non-slip boundary is drawn on the solid wall. We default the simulation to reach a steady state when the velocity change of each grid between two time steps is less than 0.0001%. Note that the fact that the isothermal boundary condition has been adopted in the above deduction.

The lattice units are used in the above-mentioned parameters. Therefore, it is necessary to convert the studied physical quantity (e.g. permeability) from the lattice unit to the physical unit. The permeability can be determined by Eq. (8) following the theoretical model of capillary model.



(a)



(b)

Fig. 3. The verification of the box-counting method. (a) is the Sierpinski Carpet image and (b) is the value estimated by the box-counting method.

$$\frac{K}{K_{LBM}} = \left(\frac{L}{L_{LBM}} \right)^2 \quad (8)$$

where K and K_{LBM} are the intrinsic permeability with physical unit and the permeability simulated by LBM, respectively. L is the real scale of coal sample and L_{LBM} is the scale of LBM. Other physical property parameters such as kinematic viscosity required for methane under different pressure and temperature conditions can be obtained from the open source software called Peace software.

2.5. Validation of Box-counting and lattice Boltzmann methods

2.5.1. Box-counting method

Sierpinski Carpet as a classic figure (as shown in Fig. 3a) in fractal theory can be used to verify the accuracy of our calculation program. The definition of fractal dimension determines Sierpinski Carpet's theoretical fractal dimension $D = \frac{\ln 8}{\ln 3} \approx 1.8928$. As presented in Fig. 3b, the actual result we calculated is also 1.8928, which indicates that the actual result is in good agreement with the theoretical value. In other words, this comparison confirms that our program is feasible.

2.5.2. Lattice Boltzmann method

The second validation is carried out by simulating the flow of two-dimensional Poiseuille with different lattice sizes including $100 \times$

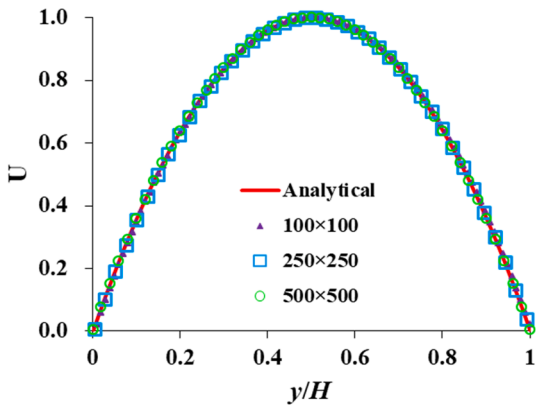


Fig. 4. Normalized streamwise velocity profiles with different lattice sizes.

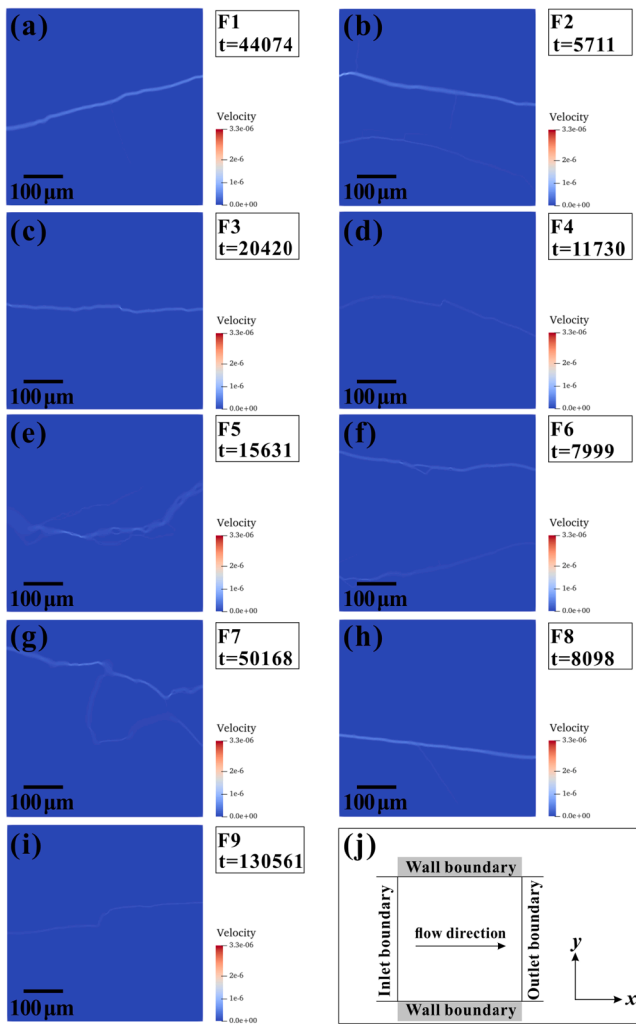


Fig. 5. The velocity distribution results of dimensionless lattice unit when the simulation reaches equilibrium with different micro-fractures morphologies and the schematic diagram of the gas flow model. t is the time for the simulation to reach convergence. (a)–(i) are the velocity distribution results and (j) is the schematic diagram of the gas flow model. Simulation conditions include $T = 300$ K, outlet pressure = 10 MPa and pressure gradient = 0.1 MPa/m.

100, 250×250 and 500×500 . The normalized streamwise velocity profiles $U = u/u_{max}$ are compared with the analytical solution as shown in Fig. 4, which shows that the simulation results based on a series of lattice sizes are highly consistent with the analytical solutions. This

Table 2

Statistics of the length and width for the dominant channel of micro-fractures in Fig. 1.

Figure ID	Fig. 1(a)	Fig. 1(b)	Fig. 1(c)	Fig. 1(h)	Average
Length (μm)	506.66	495.61	493.68	497.10	498.26
Width (μm)	13.63	10.19	11.13	8.88	10.96

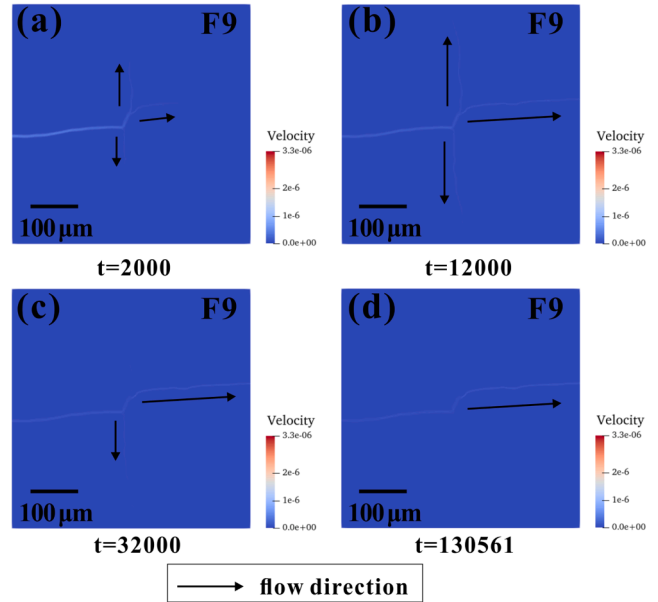


Fig. 6. Velocity distribution of sample F9 under different time steps. t is the time step. The length of the arrow indicates how far the gas flows. At the beginning of the flow process, the gas will extend in three directions after meeting the bifurcation. As time goes on, the gas will flow further following with the branches. At this time, the upward and downward flow directions do not match the main flow direction, so the gas in the up and down directions will gradually disappear. When the simulation reaches equilibrium, the gas only passes in the main flow direction. The equilibrium time also becomes longer due to the special angle (orthogonal type) of the branches of the microfracture network. Simulation conditions include $T = 300$ K, outlet pressure = 10 MPa and pressure gradient = 0.1 MPa/m.

consistency also confirms that the LBM is suitable for understanding the flow capability.

3. Results and discussion

Micro-fracture morphology, pressure and temperature are three of the important factors affecting permeability and thus enhancing CBM recovery [39–41]. This section captured the flow characteristics of methane under different micro-fractures morphologies, different pressures and temperatures based on the D2Q9 model. The pressure gradient was set to 0.1 MPa/m in the simulation along the flow direction.

3.1. Effects of micro-fracture morphology on flow capability

The pre-existing natural fractures characteristics are of importance on the hydraulic fracturing stimulation effect [7]. Herein, the effect of pre-existing natural fracture morphology on methane flow in coal will be discussed in detail. The velocity distribution results with different micro-fractures morphologies are displayed in Fig. 5 as the simulation reaches steady state (i.e. the velocity change of each grid between two time steps is less than 0.0001%). Fig. 5 demonstrates that the pressure-driven methane migration in various micro-fracture networks is different. It is easy to find out that the existence of dominant channels is conducive to the gas flow, that is, there is a wide channel connecting the

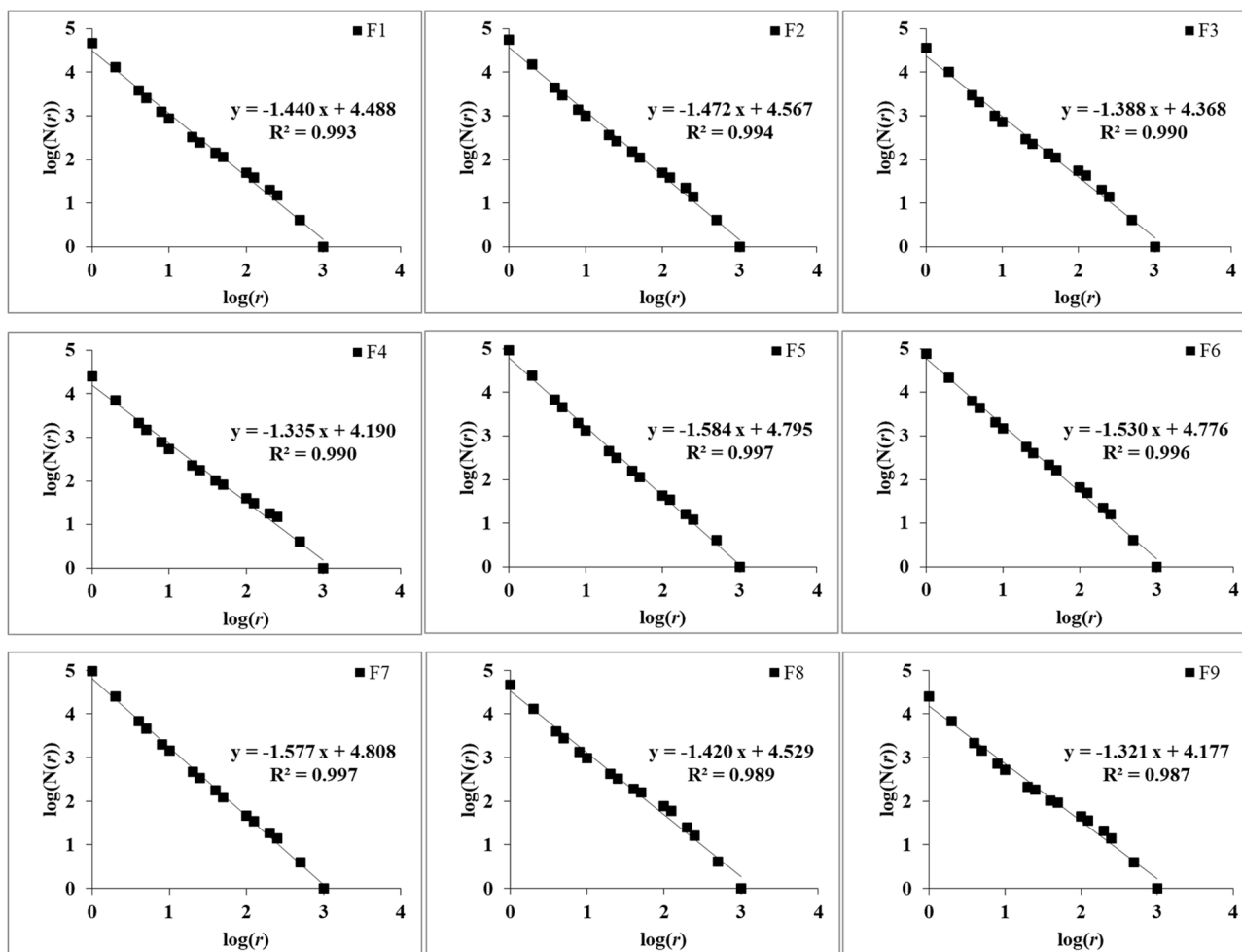


Fig. 7. Results of fractal dimension calculated by the box-counting method.

inlet to the outlet in the micro-fracture network as shown in Fig. 1. The length and width of the dominant channel was listed in Table 2, which has the average length and width of $\sim 498.26 \mu\text{m}$ and $10.96 \mu\text{m}$, respectively. The velocity in the dominant channel is much larger compared with other locations (see Fig. 5). As shown in Fig. 5d and i, gas flow is much more difficult if the micro-fracture network is connected by narrower channels with width less than $5 \mu\text{m}$. Another interesting phenomenon is that the special micro-fracture morphology determines the time that the flow simulation reaches the steady state, which varies from 5711 to 130,561 showing greatly different. This result means that the time for the simpler micro-fracture network is much shorter to reach the steady state, while the micro-fracture network with a more special shape (e.g., the orthogonal type in Fig. 5i and Fig. 6) and a more complex distribution (see Fig. 5g) takes longer to reach steady state. The equilibrium time in Fig. 5 is used as the standard to evaluate the difficulty of fluid flow in micro-fracture network, the orthogonal micro-fracture is unfavorable for flow capability, and the most favorable network is reticular. And the dendritic and filamentous types are in between the orthogonal and reticular types. The dendritic type with more branches will cause obstacles to flow. The filamentous type has a lot of narrow throats, which result in flow in filamentous structure more difficult than that in the dendritic structure with fewer branches. Fig. 6 displays the simulated flow process of the orthogonal micro-fracture network. At the beginning of the flow process, the gas will extend in three directions after meeting the bifurcation. As time goes on, the gas will flow further following with the branches. At this time, the upward and downward flow directions do not match the main flow direction; therefore, the gas in the up and down directions will gradually disappear. When the

simulation reaches the steady state, the gas only passes in the main flow direction. The computation time also becomes longer due to the special angle (e.g., orthogonal type) of the branches in the natural micro-fracture network.

The fracture dimension values calculated by BCM are displayed in Fig. 7, which ranges from 1.321 to 1.584. The larger the value is, the more complicated distribution of the natural micro-fracture network [16]. Besides, Fig. 8b reveals that there is an obvious positive correlation between the fractal dimension and the fracture porosity. This phenomenon may be ascribed to two causes: the first is that micro-fracture network with larger fracture porosity will have a greater chance of being more complicated distribution, which is consistent with Wu et al. [36]. Secondly, the micro-fracture networks in this study are rarely filled with minerals, thus there is no complex trend that is similar to the relationship between porosity and fractal dimension [35].

As shown in Fig. 8a, there is a significant inverted U-shaped relationship between fractal dimension and permeability with the correlation coefficient of 0.86. The permeability increases as fractal dimension increases from 1.321 to 1.472, and then decreases as fractal dimension exceeds 1.472. The permeability is 0.147 D when the fractal dimension is 1.321, while it increases to 0.345 D as fractal dimension reaches to 1.472. The reason for this increasing trend is that lower fractal dimension normally corresponds to lower fracture porosity, resulting in lower permeability. As the fractal dimension increases, the fracture porosity also increases, and the permeability is improved when the connectivity of the micro-fracture network is good. However, when the fractal dimension exceeds 1.472, the micro-fracture network becomes more complex. Meanwhile, due to the strong heterogeneity of the CBM

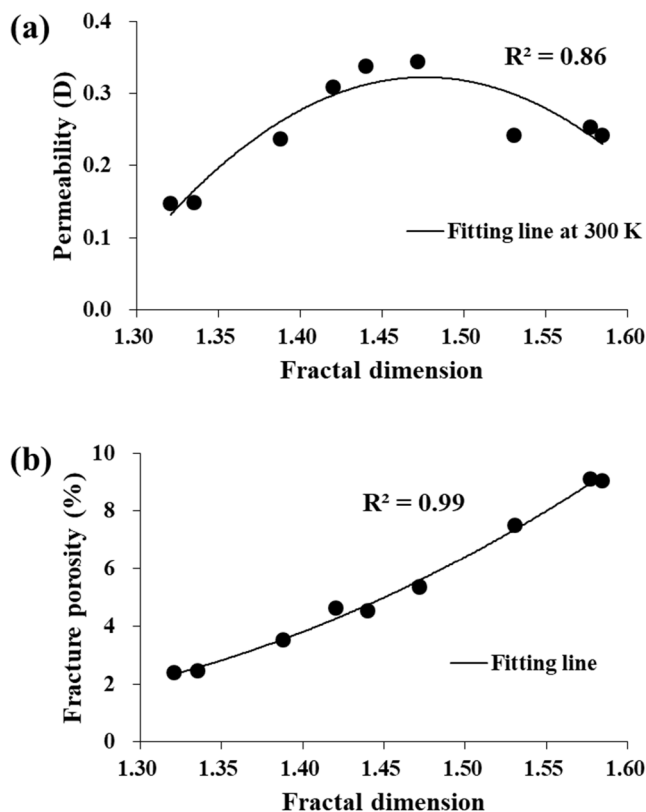


Fig. 8. Relations between permeability, fracture porosity and fractal dimension. (a) Fractal dimension versus permeability and (b) fractal dimension versus fracture porosity. $T = 300$ K, outlet pressure = 10 MPa and pressure gradient = 0.1 MPa/m.

reservoir and poor connectivity [1,26,42], the natural micro-fracture network is connected by the narrow throat, leading to difficult gas flow and thus lower permeability. Fig. 9 shows that the methane still flows through the micro-fracture network branch f1 (see f2) at the beginning of the flow process, but methane will not pass through these channels as time increases. Hence, under the premise of only one flow direction, the flow time will undoubtedly take longer if many branches exist in the micro-fracture network. And if the extension direction of these branches is different from the flow direction, it would constrain the permeability.

3.2. Effects of pressure on flow capability

The trend of permeability together with outlet pressure is shown in Fig. 10, which illustrates that the permeability decreases sharply as pressure increases from 0.1 MPa to 5 MPa, and then the permeability tends to be stable as pressure exceeds 5 MPa. In other words, the natural micro-fracture network is more sensitive to change in permeability at low pressure because the distance between the rarefied gas molecules is far away and the attractive force is weak at low pressure [29]. The decreasing trend of permeability with increasing pressure is consistent with the shale gas production [27,43]. However, when the permeability is larger than 5 MPa, there is no similar trend in CBM production by Shi and Durucan [44]. During the CBM production, the permeability initially declines and then increases with increasing pressure [6,44]. The reason for this phenomenon is that the shrinkage of the coal matrix due to gas desorption, a unique characteristic of coal reservoir, counteracts the permeability decrease with pressure drop during the production [4,45]. Therefore, a model considering matrix swelling/shrinkage can accurately describe actual flow characteristics. Due to its extremely challenging nature, coal matrix swelling/shrinkage response during gas

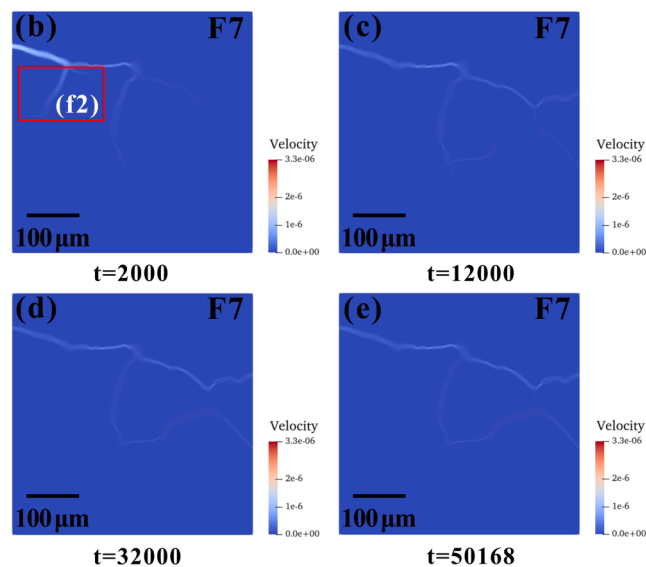
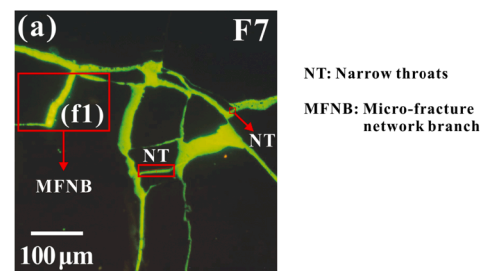


Fig. 9. Velocity distribution of sample F7 under different time steps. t is the time step. (a) is the initial image of F7 and (b)-(e) are the velocity distribution under different time steps during simulation. f1 and f2 are the original image of the branch and the changes that occurred in the branch during the flow process, respectively.

flow should be considered into the permeability model.

3.3. Effects of temperature on flow capability

Three sets of temperatures were simulated to study the effects of temperature changes including 300 K, 330 K and 360 K on coal permeability. Fig. 10 exhibits that the permeability increase with increasing temperature at the constant pressure. The increase of temperature will aggravate the thermal motion of gas molecules, leading to the average kinetic energy of the molecules increasing and thereby increasing the permeability, which is in accordance with previous research [29]. And at low pressure, the influence of temperature on permeability is more sensitive. For realistic CBM production, the effect of temperature on coal permeability is related to many factors, such as coal rank and pore-fracture structure [39,42]. For instance, Cai et al. [39] revealed that different rank coals have different trends in permeability changes caused by temperature. And Liu et al. [42] found that the temperature has obvious impact on the mechanical properties and acoustic emission characteristics in coal, and the pore-fracture structures were promoted and the permeability was significantly improved under temperature treatment. CBM reservoirs normally have the characteristics of complex pore-fracture structure, strong heterogeneity, and abundant mineral types, which cause a series of physical and chemical changes in the process of temperature increase [46]. Different components in coal have different shrinking and swelling ability under the effect of temperature [42]. For example, the temperature stress will aggravate the expansion of fractures and weaken the mechanical properties of coal [42]. Moreover, during the exploitation of CBM, the reservoir temperature also changes dynamically with produced gases;

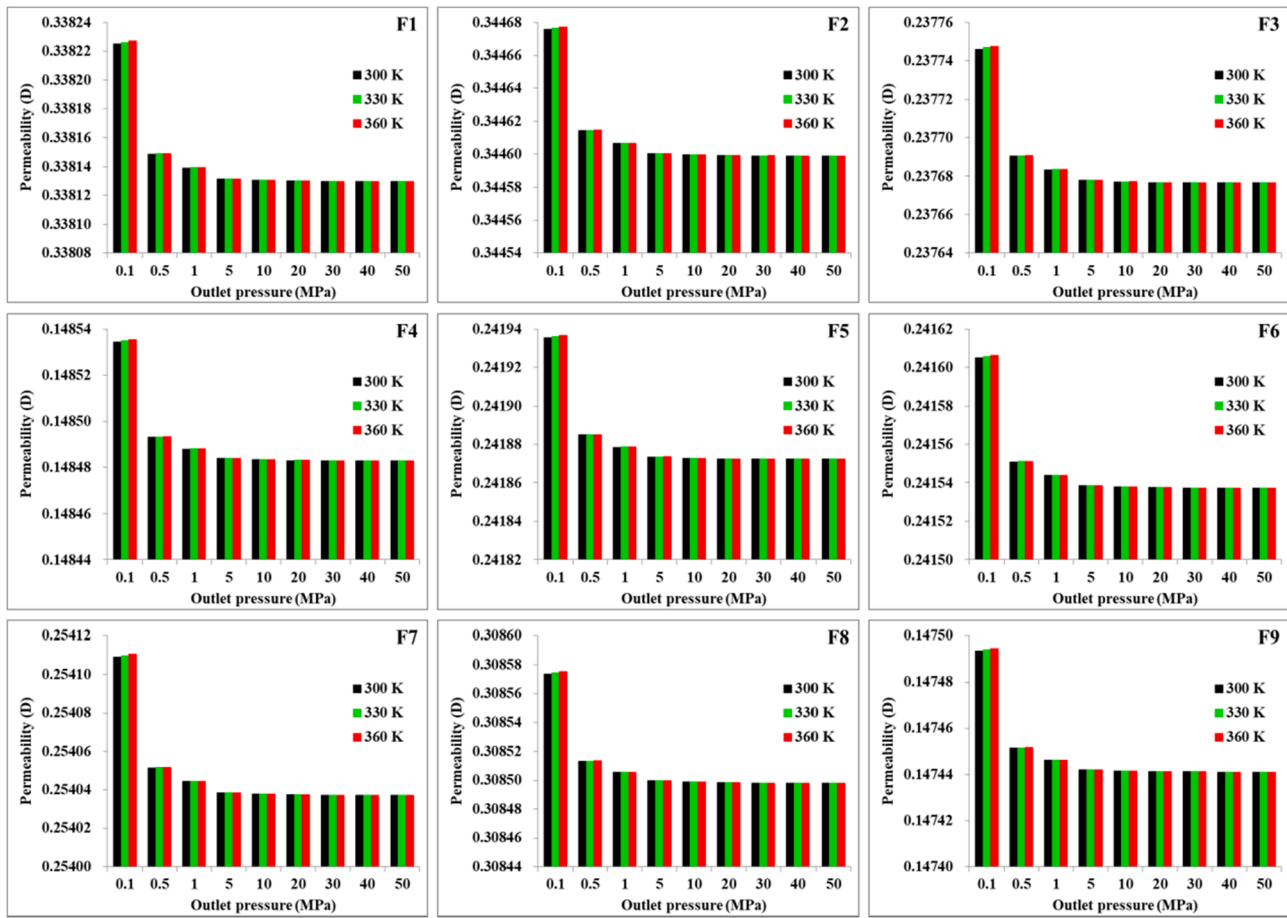


Fig. 10. Relations between pressure, temperature and permeability in different samples. Pressure gradient = 0.1 MPa/m.

thus, the effect of temperature on permeability should be cautiously considered [47]. Therefore, the micro-fracture morphology, pressure and temperature have a comprehensive complex influence on gas flow capability, which generally follows the dominated micro-fracture morphology, supplemented by pressure and temperature as shown in Fig. 11.

Although the detailed work on the morphology effect of micro-fracture network on permeability has been revealed, the process of fluid–solid coupling has yet to confirm. Therefore, the flow response in micro-nano scale natural pore-fracture structure during the CBM development will be our next work.

4. Conclusions

In this study, natural micro-fracture morphologies of selected Chinese coals from the Ordos Basin were characterized by the optical microscope. And the box-counting method together with the lattice Boltzmann method was adopted to quantify the complexity of the micro-fracture network and flow behaviors in these natural micro-fracture networks. Besides, factors affecting the flow capability in these natural micro-fracture networks were discussed. The following conclusions can be made:

1) The dominant channels in the natural micro-fracture network will greatly improve the permeability. Besides, flow characteristics in the micro-fracture networks with various morphologies are quite different, which presents that the orthogonal type is unfavorable for flow capability, and the most favorable network is reticular, with dendritic and filamentous types in between.

- 2) An obvious inverted U-shaped relationship exists between the fractal dimension and permeability. When the fractal dimension is lower than 1.472, the larger fractal dimension means the greater fracture porosity, and thus the permeability of well-connected natural micro-fractures increase. As the fractal dimension exceeds 1.472, the distribution of natural micro-fracture network is complicated, which presents reticular and dendritic types. And the connected narrow throats normally lead to a permeability decrease.
- 3) Pressure and temperature have opposite influence on coal permeability. The permeability increases with decreasing gas pressure, which is caused by the rarefied gas due to the declining pressure. However, the gas at high temperatures of 360 K will lead to a gentle increase of permeability.

CRediT authorship contribution statement

Qian Li: Writing - original draft, Investigation, Validation. **Dameng Liu:** Conceptualization, Methodology. **Yidong Cai:** Conceptualization, Funding acquisition, Supervision, Writing - review & editing. **Bo Zhao:** Validation. **Yuejian Lu:** Writing - review & editing. **Yingfang Zhou:** Writing - review & editing.

Declaration of Competing Interest

The authors declare that they have no known competing financial interests or personal relationships that could have appeared to influence the work reported in this paper.

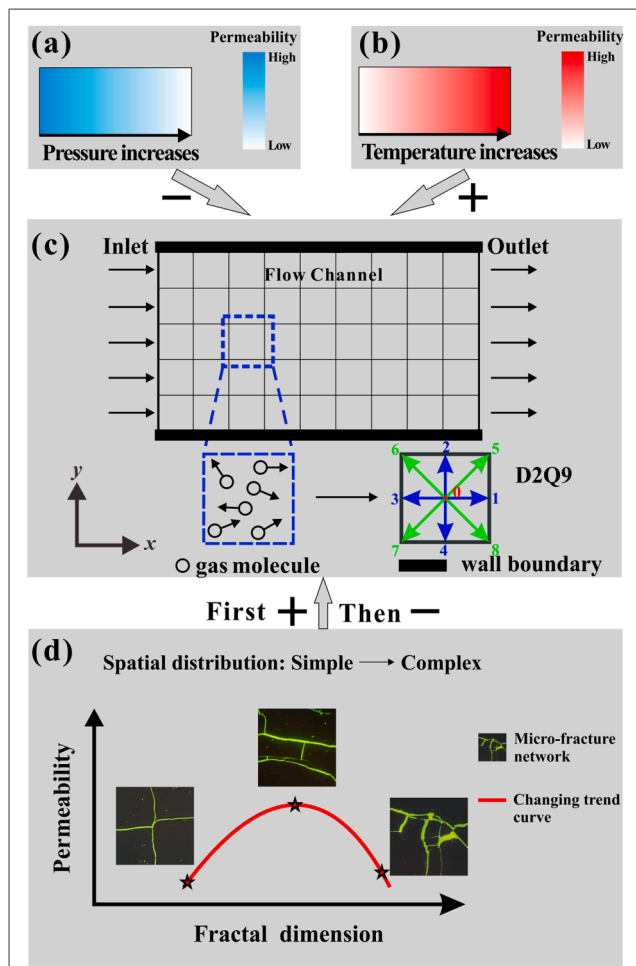


Fig. 11. Diagram of the influence mechanism of different factors on permeability, including the micro-fracture morphology, pressure and temperature. The positive and negative signs (“+” and “-”) in the figure represent the promotion and inhibition effects, respectively.

Acknowledgements

This research was funded by the National Natural Science Foundation of China (grant nos. 41830427, 41922016 and 41772160) and the Fundamental Research Funds for Central Universities (grant no. 2652019255). The authors also want to thank the Royal Society Edinburgh and NSFC to support their collaborations.

References

- [1] Moore TA. Coalbed methane: A review. *Int J Coal Geol* 2012;101:36–81.
- [2] Vishal V, Singh TN, Ranjith PG. Influence of sorption time in CO₂-ECBM process in Indian coals using coupled numerical simulation. *Fuel* 2015;139:51–8.
- [3] Jia D, Qiu Y, Li C, Cai Y. Propagation of pressure drop in coalbed methane reservoir during drainage stage. *Adv. Geo-Energ. Res.* 2019;3(4):387–95.
- [4] Cai Y, Li Q, Liu D, Zhou Y, Lv D. Insights into matrix compressibility of coals by mercury intrusion porosimetry and N₂ adsorption. *Int J Coal Geol* 2018;200:199–212.
- [5] Laubach SE, Marrett RA, Olson JE, Scott AR. Characteristics and origins of coal cleat: A review. *Int J Coal Geol* 1998;35(1-4):175–207.
- [6] Pan Z, Connell LD. Modelling permeability for coal reservoirs: A review of analytical models and testing data. *Int J Coal Geol* 2012;92:1–44.
- [7] Yao W, Mostafa S, Yang Z, Xu G. Role of natural fractures characteristics on the performance of hydraulic fracturing for deep energy extraction using discrete fracture network (DFN). *Eng Fract Mech* 2020;230:106962.
- [8] Zheng S, Yao Y, Liu D, Cai Y, Liu Y. Nuclear magnetic resonance surface relaxivity of coals. *Int J Coal Geol* 2019;205:1–13.
- [9] Harmer J, Callcott T, Maeder M, Smith BE. A novel approach for coal characterization by NMR spectroscopy: global analysis of proton T₁ and T₂ relaxations. *Fuel* 2001;80(3):417–25.
- [10] Mathews JP, Campbell QP, Xu H, Halleck P. A review of the application of X-ray computed tomography to the study of coal. *Fuel* 2017;209:10–24.
- [11] Balucan RD, Turner LG, Steel KM. X-ray mu CT investigations of the effects of cleat demineralization by HCl acidizing on coal permeability. *J Nat Gas Sci Eng* 2018;55:206–18.
- [12] Jenkins DR, Lomas H, Mahoney M. Uniaxial compression of metallurgical coke samples with progressive loading. *Fuel* 2018;226:163–71.
- [13] Cai Y, Liu D, Pan Z, Che Y, Liu Z. Investigating the effects of seepage-pores and fractures on coal permeability by fractal analysis. *Transp Porous Med* 2016;111(2):479–97.
- [14] Mahnke M, Mögel HJ. Fractal analysis of physical adsorption on material surfaces. *Colloids Surf A* 2003;216(1-3):215–28.
- [15] Peng C, Zou C, Yang Y, Zhang G, Wang W. Fractal analysis of high rank coal from southeast Qinshui basin by using gas adsorption and mercury porosimetry. *J Petrol Sci Eng* 2017;156:235–49.
- [16] Liu X, Nie B. Fractal characteristics of coal samples utilizing image analysis and gas adsorption. *Fuel* 2016;182:314–22.
- [17] Lopes R, Betrouni N. Fractal and multifractal analysis: A review. *Med Image Anal* 2009;13(4):634–49.
- [18] Liu P, Qin YP, Liu SM, Hao YJ. Modeling of gas flow in coal using a modified dual-porosity model: a multi-mechanistic approach and finite difference method. *Rock Mech Rock Eng* 2018;51(9):2863–80.
- [19] Sun Z, Logé RE, Bernacki M. 3D finite element model of semi-solid permeability in an equiaxed granular structure. *Comput Mater Sci* 2010;49(1):158–70.
- [20] Almasoodi M, Reza Z. Finite-volume computations of shale tortuosity and permeability from 3D pore networks extracted from scanning electron tomographic images. *Petro S J* 2019;60(3):397–408.
- [21] Aidun CK, Clausen JR. Lattice-Boltzmann method for complex flows. *Annu. Rev. Fluid Mech.* 2010;42(1):439–72.
- [22] Liu H, Kang Q, Leonardi CR, Schmieschek S, Narváez A, Jones BD, Williams JR, Valocchi AJ, Harting J. Multiphase lattice Boltzmann simulations for porous media applications: A review. *Comput Geosci* 2016;20(4):777–805.
- [23] Wang M, Chen Y-F, Ma G-W, Zhou J-Q, Zhou C-B. Influence of surface roughness on nonlinear flow behaviors in 3D self-affine rough fractures: Lattice Boltzmann simulations. *Adv Water Resour* 2016;96:373–88.
- [24] Zhao Y-L, Wang Z-M, Ye J-P, Sun H-S, Gu J-Y. Lattice Boltzmann simulation of gas flow and permeability prediction in coal fracture networks. *J Nat Gas Sci Eng* 2018;53:153–62.
- [25] Zhao Y-L, Wang Z-M, Qin X, Li J-T, Yang H. Stress-dependent permeability of coal fracture networks: A numerical study with Lattice Boltzmann method. *J Petrol Sci Eng* 2019;173:1053–64.
- [26] Jing Yu, Armstrong RT, Mostaghimi P. Image-based fracture pipe network modelling for prediction of coal permeability. *Fuel* 2020;270:117447.
- [27] Wang J, Kang Q, Chen L, Rahman SS. Pore-scale lattice Boltzmann simulation of micro-gaseous flow considering surface diffusion effect. *Int J Coal Geol* 2017;169:62–73.
- [28] Gupta N, Fathi E, Belyadi F. Effects of nano-pore wall confinements on rarefied gas dynamics in organic rich shale reservoirs. *Fuel* 2018;220:120–9.
- [29] Yuan Y, Wang Y, Rahman SS. Reconstruction of porous structure and simulation of non-continuum flow in shale matrix. *J Nat Gas Sci Eng* 2017;46:387–97.
- [30] Yao Y-B, Liu D-M. Microscopic characteristics of microfractures in coals: an investigation into permeability of coal. *Procedia Earth Planet Sci* 2009;1(1):903–10.
- [31] International Committee for Coal and Organic Petrology (ICCP). The new vitrinite classification (ICCP System 1994). *Fuel* 1998;77(5):349–58.
- [32] Zhou HW, Xie H. Direct Estimation of the Fractal Dimensions of a Fracture Surface of Rock. *Surf. Rev. Lett.* 2003;10(05):751–62.
- [33] Mandelbrot BB, Wheeler JA. The fractal geometry of nature. *Am J Phys* 1983;51(3):286–7.
- [34] Ai T, Zhang R, Zhou HW, Pei JL. Box-counting methods to directly estimate the fractal dimension of a rock surface. *Appl Surf Sci* 2014;314:610–21.
- [35] Li Q, Liu D, Cai Y, Zhao B, Qiu Y, Zhou Y. Scale-span pore structure heterogeneity of high volatile bituminous coal and anthracite by FIB-SEM and X-ray μ -CT. *J Nat Gas Sci Eng* 2020;81:103443.
- [36] Wu H, Zhou Y, Yao Y, Wu K. Imaged based fractal characterization of micro-fracture structure in coal. *Fuel* 2019;239:53–62.
- [37] Bhatnagar PL, Gross EP, Krook M. A model for collision processes in gases. I. Small amplitude processes in charged and neutral one-component systems. *Phys. Rev.* 1954;94(3):511–25.
- [38] Qian YH, D’Humières D, Lallemand P. Lattice BGK models for Navier-stokes equation. *Europhys. Lett.* 1992;17(6):479–84.
- [39] Cai Y, Pan Z, Liu D, Zheng G, Tang S, Connell LD, Yao Y, Zhou Y. Effects of pressure and temperature on gas diffusion and flow for primary and enhanced coalbed methane recovery. *Energy Explor Exploit* 2014;32(4):601–19.
- [40] Wang G, Han D, Jiang C, Zhang Z. Seepage characteristics of fracture and dead-end pore structure in coal at micro- and meso-scales. *Fuel* 2020;266:117058.
- [41] Mostaghimi P, Armstrong RT, Gerami A, Hu Y, Jing Yu, Kamali F, Liu M, Liu Z, Lu X, Ramandi HL, Zamani A, Zhang Y. Cleat-scale characterisation of coal: An overview. *J Nat Gas Sci Eng* 2017;39:143–60.
- [42] Liu S, Li X, Wang D, Wu M, Yin G, Li M. Mechanical and acoustic emission characteristics of coal at temperature impact. *Nat Resour Res* 2020;29(3):1755–72.
- [43] Cui G, Liu J, Wei M, Shi R, Elsworth D. Why shale permeability changes under variable effective stresses: New insights. *Fuel* 2018;213:55–71.
- [44] Shi JQ, Durucan S. Exponential growth in San Juan Basin Fruitland coalbed permeability with reservoir drawdown: Model match and new insights. *Spe Reserv Eval Eng* 2010;13(6):914–25.

- [45] Gray I. Reservoir engineering in coal seams: part 1-The physical process of gas storage and movement in coal seams. SPE-12514-PA 1987;2(01):28-34.
- [46] Sharma A, Kyotani T, Tomita A. Quantitative evaluation of structural transformations in raw coals on heat-treatment using HRTEM technique. Fuel 2001;80(10):1467-73.
- [47] Liu S, Wei C, Zhu W, Zhang M. Temperature- and pressure-dependent gas diffusion in coal particles: Numerical model and experiments. Fuel 2020;266:117054.